Design of Protein-Based Liquefied Cell-Laden Capsules with Bioinspired Adhesion for Tissue Engineering

COMPASS

ENGINEERING LIFE GUIDED BY NATURE

This paper must be cited as: Gomes, M. C., Costa, D. C., Oliveira, C. S., & Mano, J. F. Design of Protein-Based Liquefied Cell-Laden Capsules with Bioinspired Adhesion for Tissue Engineering. 10(19), 2100782. Advanced Healthcare Materials, (2021). https://doi.org/https://dx.doi.org/10.1002/adhm.202100782

Design of protein-based liquified cell-laden capsules with bioinspired adhesion for tissue engineering

Maria C. Gomes, Dora C. S. Costa, Cláudia S. Oliveira, João F. Mano**

Dr. M. C. Gomes, Dr. D. C. S. Costa, Dr. C. S. Oliveira, Prof. J. F. Mano
Department of Chemistry, CICECO-Aveiro Institute of Materials
University of Aveiro
Campus Universitário de Santiago
3810-193 Aveiro, Portugal
E-mail: clara.gomes@ua.pt, jmano@ua.pt

Keywords: cell encapsulation, hydroxypyridinones, superhydrophobic surfaces, 3D assembly

Platforms with liquid cores are extensively explored as cell delivery vehicles for cell-based therapies and tissue engineering. However, the recurrence of synthetic materials can impair its translation into the clinic. Inspired by the adhesive proteins secreted by mussels, liquefied capsule is developed using gelatin modified with hydroxypyridinones (Gel-HOPO), a catechol analogue with oxidant-resistant properties. The protein-based liquefied macrocapsule permitted the compartmentalization of living cells by an approachable and non-time-consuming methodology resorting to i) superhydrophobic surfaces as a processing platform of hydrogel beads, ii) gelation of gelatin at temperatures < 25 °C, iii) iron coordination of the hydroxypyridinone (HOPO) moieties at physiological pH, and iv) core liquefaction at 37 °C. With the design of a proteolytically degradable shell, the possibility of encapsulating human adipose-derived mesenchymal stem cells (hASC) with and without the presence of polycaprolactone microparticles (μPCL) is evaluated. Showing prevalence toward adhesion to the inner shell wall, hASC formed a monolayer evidencing the biocompatibility and adequate mechanical properties of these platforms for proliferation, diminishing the need for

μPCL as a supporting substrate. This new protein-based liquefied platform can provide biofactories devices of both fundamental and practical importance for tissue engineering and regenerative medicine or in other biotechnology fields.

1. Introduction

The engineering of new tissues exploiting cutting-edge bottom- up based strategies leads cell encapsulation in liquid environments toward the latest generation.[1] Upholding superior multi- functionality, liquid environments can be fabricated under mild conditions providing cell containment and protection while offering higher nutrient diffusion.[2] The increased knowledge be- hind the cellular microenvironment complexity and the possibility of better mimic the native physical and biochemical cues make the choice of the biomaterials critical in the design of high-class platforms.[3] Up to date, a wide variety of polymers (synthetic and natural), biofabrication technologies (e.g., electrospray, microfluidic, among others) and approaches (e.g., layer-by-layer, aqueous biphasic systems) are underneath the design of a shell confinement (i.e., a barrier able to confine cells in a controlled environment).[4–9] However, most of those systems resort to the com- bination of synthetic and natural polymers to create cell confinement, limiting its translation into the clinic. Although these approaches can engineer self-organized microtissues with the cells enclosed in a semi- permeable shell, as most mammalian cells require a solid matrix for attachment, the inclusion of synthetic microcarriers (e.g., microparticles) is sometimes required.[10]

Over the years, proteins have earned their spotlight as promising biomaterials for tis- sue engineering, with gelatin (a collagen degradation product) the most chemically tailored and explored protein.[11] The inclusion of proteins as shell building blocks can offer proteolytic degradability, allowing the newly deposited extracellular matrix (ECM) to

replace the native shell, promoting an ap- propriate tissue integration.[12] In addition, proteins proved to be suitable for chemical modifications as natural polymers, with a plethora of chemical motifs already tailored in their backbone.[13] Inspired by nature, scientists succeeded to mimic the strong adhesion ability showed by mussels in wet environments with the introduction of catechol analogue molecules, resembling the amino acid responsible for such ability (3,4-dihydroxy-L-phenylalanine, L-DOPA).[14,15] The most acknowledged catechol analogue is dopamine, already used to tailor gelatin (among several synthetic and natural polymers) yielding subtract adhesives or injectable hydrogels, among others.[16–18] However, the coordination degree appears to be pH-dependent, with the most stable coordination (tris) only achieved at basic pH (>8.0), occurring at the same pH spontaneous oxidation resulting in species unable to coordinate. Impairing the use of dopamine in physiological conditions, synthetic catechol- like derivative molecules such as hydroxypyridinones (HOPO) have emerged, allowing to achieve maximum coordination un- der physiologic pH.[19,20]

In this study, we showcase an approachable and straight- forward methodology yielding biologically active liquefied macrosystems resorting to the coordination behavior of the HOPO moieties tailored in the gelatin side chains. By designing a protein-based hydrogel shell with controllable thickness, we combined the mechanical properties of hydrogels with the benefits of liquefied environments, upgrading the cell confinement environment. Compared to classical approaches, this offers a functional superiority promoting the diffusion of nutrients and cell waste while allowing cell adhesion, proliferation and partial self-organization within the capsule, even in the absence of microparticles as cell carries. We hypothesize that such capsules could be used as building blocks to engineering devices at a larger scale, suitable for applications such as in the regeneration of damaged tissues.

2. Results and Discussion

2.1. Optimal Conditions for the Biofabrication of Protein-Based Liquefied Capsules

The novel biomaterial functionalized with oxidation-resistant catechol-like moieties, gelatin-HOPO (Gel-HOPO), was prepared following the synthetic pathway outlined in Figure 1A. HOPO- NH_2 was obtained as a light brown solid in 54% yield by direct condensation of maltol with ethylenediamine (EDA). The ^1H NMR spectrum (Figure S1B, Supporting Information) shows one singlet at 2.42 ppm corresponding to methyl group protons (H-7); two triplets at 3.41 ppm (J = 6.8 Hz) and 4.41 ppm (J = 6.8 Hz) corresponding to the four methylene protons (H-2′ and H-3′), which confirms the condensation reaction success. At the aromatic region, we can observe two doublets at 6.51 (J = 7.3 Hz) and 7.65 (J = 7.3 Hz), characteristic of aromatic ring protons (H-5 and H-6), confirming the HOPO formation. Once HOPO- NH_2 can exhibit two different tautomers (Figure S2A, Supporting Information), depending on its ability to protonate or deprotonate the oxygen atoms, we studied its pH-responsiveness behavior by NMR. Scrutinizing the ^{13}C NMR spectrum of HOPO- NH_2, recorded at acidic conditions (Figure S2B, Supporting In- formation), it showed that under this pH (≈2.0) we only have 3,4-dihydroxy tautomer, once there was no characteristic ketone carbon signal observed. On the other hand, ^{13}C NMR spectra performed at pH ≈7.0 and pH ≈10.0 (Figure S2C,D, respectively, Supporting Information) confirmed the existence of only 3-Hydroxy-4-ceto form, showing just one characteristic ketone carbon signal at 169.5 and 170.7 ppm, respectively. HOPO has electron-withdrawing substituent groups, resulting in a lower electron density on its oxygen atoms by inductive and resonance withdrew effects, meaning a lower susceptibility to lose electrons (oxidize) than traditional catechol.

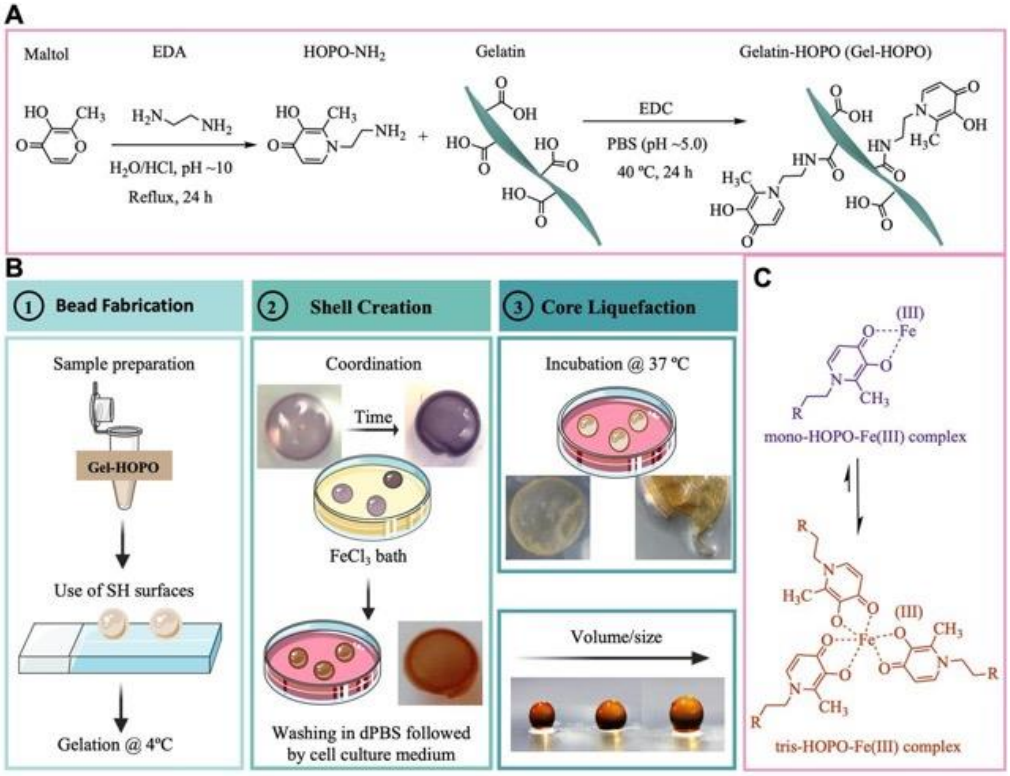

Figure 1. A) Synthetic route for the preparation of Gel-HOPO. B) Fabrication process to obtain liquefied protein-based macrocapsules with different sizes, using superhydrophobic (SH) as supporting platforms. After producing the Gel-HOPO beads, the shell is created by the coordination of HOPO with the Fe(III). Upon transference to cell culture media and incubation at 37 °C, non-coordinated gelatin dissolves, yielding liquefied protein-based macrocapsules. C) Equilibrium between mono- (purple) and tris- (orange) HOPO-Fe(III) complex structures by increasing the pH.

Simultaneously, this electron withdrawal effect favors the enolate formation once the oxygen atom has less hydrogen affinity, lowering the phenolic pKa values (HOPO: pKa_1 = 3.6, pKa_2 = 9.9; DOPA: pKa_1 = 9.1, pKa_2 = 14) what makes HOPO more resistant to oxidation than DOPA.[19] Afterward, type A gelatin was modified with HOPO moieties by EDC coupling chemistry. Gel-HOPO was obtained as a white solid with a substitution degree of 2.1% w/w (6.8 μg mL^{-1}) con- firmed by UV–Vis spectroscopy (Figure S3,

Supporting Information). By comparing the ^{1}H NMR spectra between HOPO, pristine and modified protein (Figure S4, Supporting Informa- tion), we positively identified four new doublets at 6.69 ppm (J=7.0Hz),6.80ppm(J=7.8Hz),7.75ppm(J=7.0Hz) and 7.97 ppm (J = 7.8 Hz), characteristic signals of HOPO aromatic protons (H-5 and H-6). These two sets of doublets confirm the successful insertion of HOPO moieties while suggests a modification in two chemical environments. We hypothesize that both carboxylic terminal side chains residues and C-terminus took an active role in the achieved modified gelatin.

We combined the properties of superhydrophobic surfaces (SH) and the gelling ability of gelatin at low temperatures,[21] with the coordination efficiency of HOPO with $FeCl_3$ to fabricate the protein-based capsules (Figure 1B1). By controlling the incubation time in the $FeCl_3$ solution, we could spatially control the Fe(III) diffusion within the Gel-HOPO bead, with an increase of the violet coloration observed over time (Figure 1B2). Looking more closely, we can see a darker area outlining the bead guiding us toward the complexation of HOPO with Fe(III). Interestingly, after transferring to the cell culture media (α-MEM) the beads changed their coloration to orange, which can be related to the pH change from pH ≈6.0 ($FeCl_3$ bath) to 7.4 (culture media). It is acknowledged that iron complexes are strongly colored due to the interaction of the iron d-electronic states with the ligands, enabling the color changing from mono- (purple) to tris-complex (orange) by increasing the pH (Figure 1C).[20] In our case, HOPO moieties act as strong bidentate ligands (*i.e.,* each HOPO molecule has two coordination points) with a strong C═O oxo group and a $C{-}O^{-}$ oxyanion group. The HOPO-Fe(III) complexes are established by coordination bonds between the electrons of these two coordination groups and the unoccupied molecular orbital of Fe(III), in a octahedral arrangement (Figure 1C).[22,23] Comparing with other systems with the same type of shell design (e.g., hydrogel), this

methodology does not re- quire the use of more complex apparatus such as microfluidic or electrospray.[24,25] After forming the coordinated shell, Gel- HOPO beads were incubated at 37 °C, where the non-coordinated proteins were dissolved, yielding liquefied capsules (Figure 1B3). Differing from the systems that use alginate as sacrificial core,[26] gelatin liquefaction at physiological temperatures enables this step to be performed in vivo after implantation. This easily made- up methodology allows control over the bead size by changing the volume dropped on top of the SH surface, with size ranges between 1 to 3 mm easily achieved without losing the overall spherical shape.

2.2. Characterization of the Morphology and Adhesion Profile of the Liquefied Capsules

To achieve a stable platform for cell encapsulation purposes, we exposed the Gel-HOPO beads for different periods (4, 6, and 8 min) to a $FeCl_3$ solution, tracking the coordinated shell formation by optical microscopy (Figure 2A1). With increased exposure to Fe(III) (Figure 2A1, bracket, and 2A2), we were able to manipulate the shell thickness easily. However, incubation of the liquefied capsules at 37 °C for 240 min seems to impact the shell thickness, suggesting a deswelling phenomenon that results in shells with thickness between 22 and 26 μm (Figure 2A2). Created by the coordination of Gel-HOPO with Fe(III), the shell is a micrometer-sized hydrogel that becomes more exposed to the surrounding environment with the core liquefaction at 37 °C. Other systems have presented this same de-swelling effect when incubated in aqueous solutions,[27] this being attributed to a higher concentration of ions in the enclosing environment or due to the presence of the hydrophobic groups, represented in our case by the presence of HOPO moieties. However, no further significant differences were observed over 14 days of incubation at 37 °C, suggesting that with the deswelling of the hydrogel shell, the Gel-

HOPO establish a stable network with the Fe(III) (tris- complex).[20] These alterations in the shell were also accompanied by an expansion of the liquefied core with no changes in the overall size, proposing that this redesigning was carried out by the deswelling of the micrometer-sized hydrogel shell. Another important aspect is robustness of the yielded liquefied capsules, affecting its use in applications that require any kind of maneuver (e.g., handling, or dynamic conditions). It was observed that with only 4 min of incubation in the $FeCl_3$ solution, capsules were too fragile for handling after core liquefaction. In opposite, 6 and 8 min of incubation in the $FeCl_3$ solution considerably improved the handling robustness. Targeting protein-based capsules combining an excellent liquefied capacity for cells to grow and proliferate, with easy handling and short fabrication time, led us to select the 6 min exposure time to the $FeCl_3$ condition.

One of the critical features for the success of these platforms when aiming cell encapsulation is the permeability toward the influx of oxygen, nutrients, and growth factors essential for cell growth and proliferation. Due to the composition of the shells (hydrogels) we believe that the inflow of oxygen will be carried out by the passive diffusion from the ambient air throughout the spaces between macromolecular chains meshes.[2] Moreover, the achieved shell thickness (≈25 μm) is in accordance with the distance range known to efficiently diffuse oxygen and nutrients (≈200 μm). In a first approach, a good influx of small molecules was perceived by the pink color obtained with overnight incubation in cell culture medium at 37 °C (Figure 2B1). This coloration is derived from a small molecule (red phenol, ≈300 g mol^{-1}), indicating that other small biomolecules present in the culture media (such as amino acids, sugars, vitamins, among others) and essential for cell metabolism, can also be able to diffuse through the hydrogel shell. To better understand the permeability of the micro- sized shell we assessed the release of fluorescein isothiocyanate (FITC)-dextran. This highly stable fluorescent probe

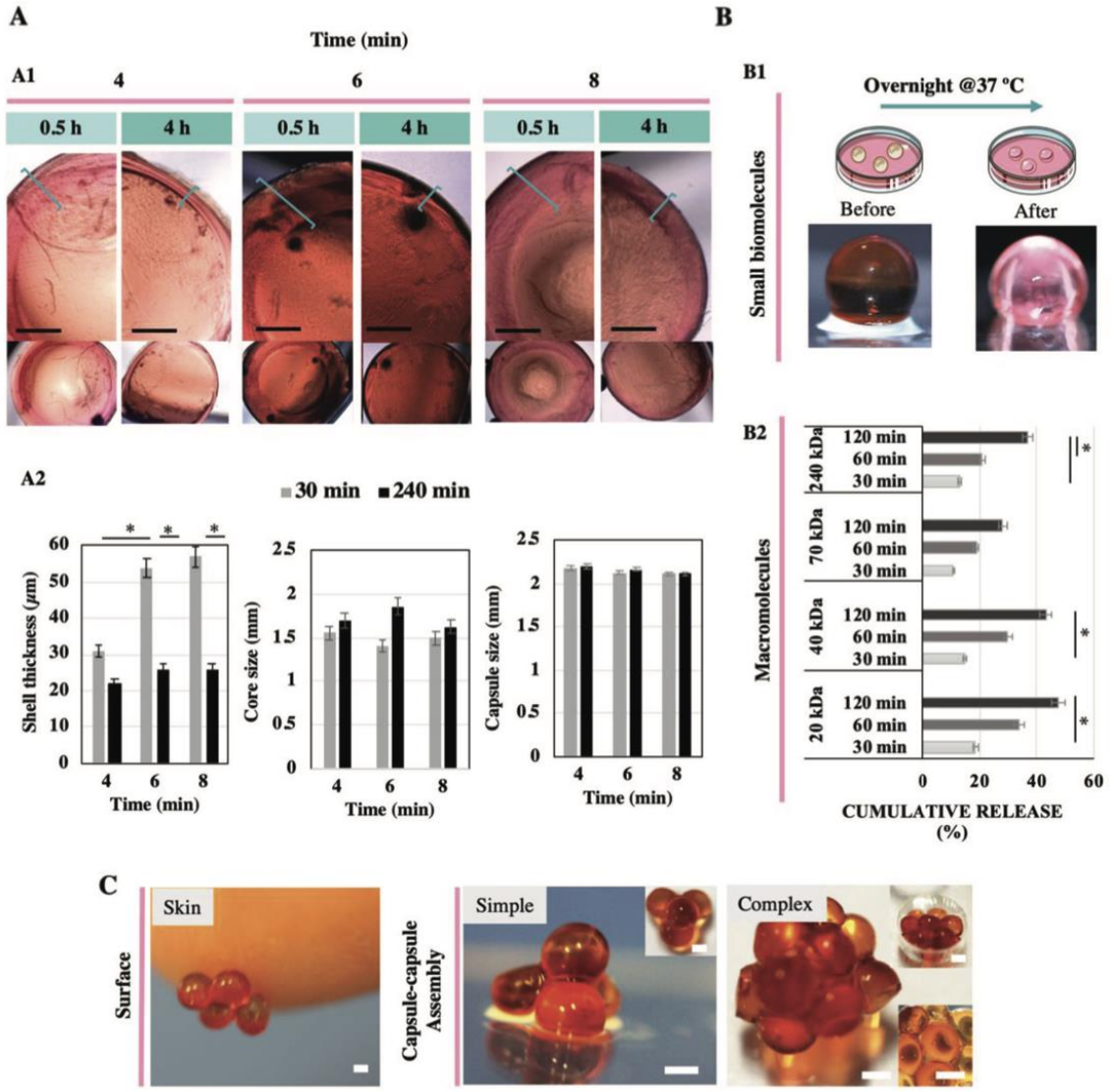

Figure 2. A) Evaluation of the morphology of the liquefied capsules after coordination in the $FeCl_3$ during different time periods and incubated at 37 °C for 30 and 240 min. A1) Optical microscopy showing the morphological changes under the different conditions. A2) Showcase comparing the different morphologies over different coordination times and evaluating the shell thickness, core, and capsule size. Results presented as means ± SD, n = 8 replicates. B) Evaluation of the shell permeability toward different constituents: B1) small molecules, and B2) different sizes of fluorescent-labeled dextran (20, 40, 70, and 240 kDa). Results are presented as means ± SD; n = 5 replicates. C) Adhesive properties conferred by the presence of HOPO in the liquefied capsules. Adhesive properties to the skin and 3D assembly ability in simple and complex constructs. Scale bar 1 mm. Statistical analysis was performed by two-way ANOVA with Tukey's post-test; statistically significant considered for * $p < 0.05$.

commonly used in these models of study, able to cover a wide range of molecular weights.[28] In this sense, the release of FITC-dextran with molecular weights ranging from 20 to 240 kDa was evaluated over time (Figure 2B2). Since early incubation times, all the tested sizes exhibited the ability to diffuse across the shell with cumulative behavior over time. The high release of small FITC-dextran molecules (20 kDa) endorses the efficiency of these liquefied capsules in diffusing essential biomolecules for cell growth, as observed with phenol red inflow. Although smaller sizes diffused in higher amounts when compared to the larger ones during the first 2 h, we believe that over time the diffusion will be total and bidirectional. These results enlighten the efficiency of these plat- forms as potential cellular containers, allowing continuous diffusion of essential molecules for cell proliferation, making possible the intercommunication with the native tissue, creating an adequate semi-closed environment to coordinate physiological functions such as proper differentiation.[29]

The presence of catechol-like molecules in the gelatin side chains opens the possibility to explore its adhesive properties onto several surfaces (organic and inorganic).[30,31] To perceive the potential of these macrocapsules in adherence to tissues or to construct 3D structures, we conducted easy-made studies (Figure 2C). Adhesion to tissues is known to be complex, requiring the complete oxidation of the catechol analogues for the covalent crosslink with amino acids (e.g., lysine and cysteine) occur.[30] In our case, HOPO cannot fully oxidize, which can hinder such interaction. Nonetheless, it still shows mild adhesions toward the skin even under gravity. Adhesion be- tween capsules is also an exciting feature allowing the assembly of these elements into a more organized construct. By simply piling the capsules or resorting to polydimethylsiloxane (PDMS) molds, we could fashion simple or more com- plex constructs without the need for external help such as external coatings, crosslinkers, or pH changes.[32–34] This capsule-capsule interaction

can be a valuable asset when aiming to create macro-tissues by a bottom-up approach, powering intercellular communication.[1]

2.3. Encapsulation of hASC

After the successfully fabrication of protein-based liquefied capsules, we evaluated the before mentioned conditions in terms of encapsulation efficiency and biocompatibility of human adipose-derived mesenchymal stem cells (hASC). As previous reports acknowledged the need for physical support when using anchorage-dependent cells in liquefied systems, we included collagen-coated polycaprolactone microparticles (μPCL) and compared cells behavior with and without its presence. After encapsulated in the Gel-HOPO beads (pre-liquefied system), hASC presents a random and homogeneous distribution in both systems with an evident migration toward the bottom when incubated at 37 °C, indicative of the core liquefaction (Figure S5A,B, Supporting Information). By analyzing the cell mem- brane integrity, we observe that up to 14 d post-encapsulation, the majority of cells remain viable for both platforms (Figure 3A1,B1), supporting the mild conditions of the encapsulation process and evidence about the ability of these protein-based capsules for long-term cell survival and proliferation. These results are accompanied by an increase in the proliferation and dispersion of living cells within the capsules when compared to shorter encapsulation periods (1 and 7 d post-encapsulation, Figure S6A, Supporting Information), providing evidence about a higher metabolic activity in the capsules without the μPCL since 1 d post-encapsulation, with an increase over time (Figure S6B, Supporting Information).

Led by the distinctive cell distribution observed between both conditions, with cells revealing a more uniform distribution without the presence of the μPCL, we evaluated the interactions between hASC and the capsule through the F-actin staining and presence

of vinculin. The staining of the F-actin microfilaments revealed that capsules with μPCL presented two distinctive patterns, one indicating the adherence to and recruitment of the microparticles by the cells, and other more elongated and through- out the capsule with no evident interaction with the μPCL (Figure 3A2), suggesting the sensing of two specific substrates. On the other hand, capsules without μPCL presented well-defined and elongated F-actin microfilaments spread throughout the capsule (Figure 3B2). Regarding vinculin expression, both environments (with and without μPCL) conduced cells to express this focal adhesion protein, indicative of key mechanosensing signals inside both capsules.[35]

We constructed a 3D image of part of each capsule (with and without μPCL) to spatially visualize the distribution of the cells within this liquefied environment. As shown by Figure 3A3,B3, there is a clear interaction of the cells with the inner wall of the shell with them recruiting and spreading along with it, fashioning virtually a second layer. These observations enlighten the presence of well-defined and elongated F-actin microfilaments. On the other hand, capsules containing μPCL provided an extra surface for cells to adhere, added by the presence of a 3D aggregate (Figure 3A3 square and S7A Supporting Information). As already stated, some liquefied platforms are enriched with the inclusion of microparticles as cell adhesion substrates.[9,10] In our specific case, the micro-sized hydrogel shell by itself seems to provide both ECM-mimic adhesion motifs and suitable mechanical cues for cell growth and proliferation, without evident formation of cellular aggregates.

Capsules without μPCL revealed the presence of cells in the outer wall of the shell after 14 d post-encapsulation, as can be observed by the presence of green fluorescence (from F-actin staining) outside the shell wall (Figure S5B3 and S7B, Supporting Information). Considering the direct interaction observed between cell/shell and the shell constitution

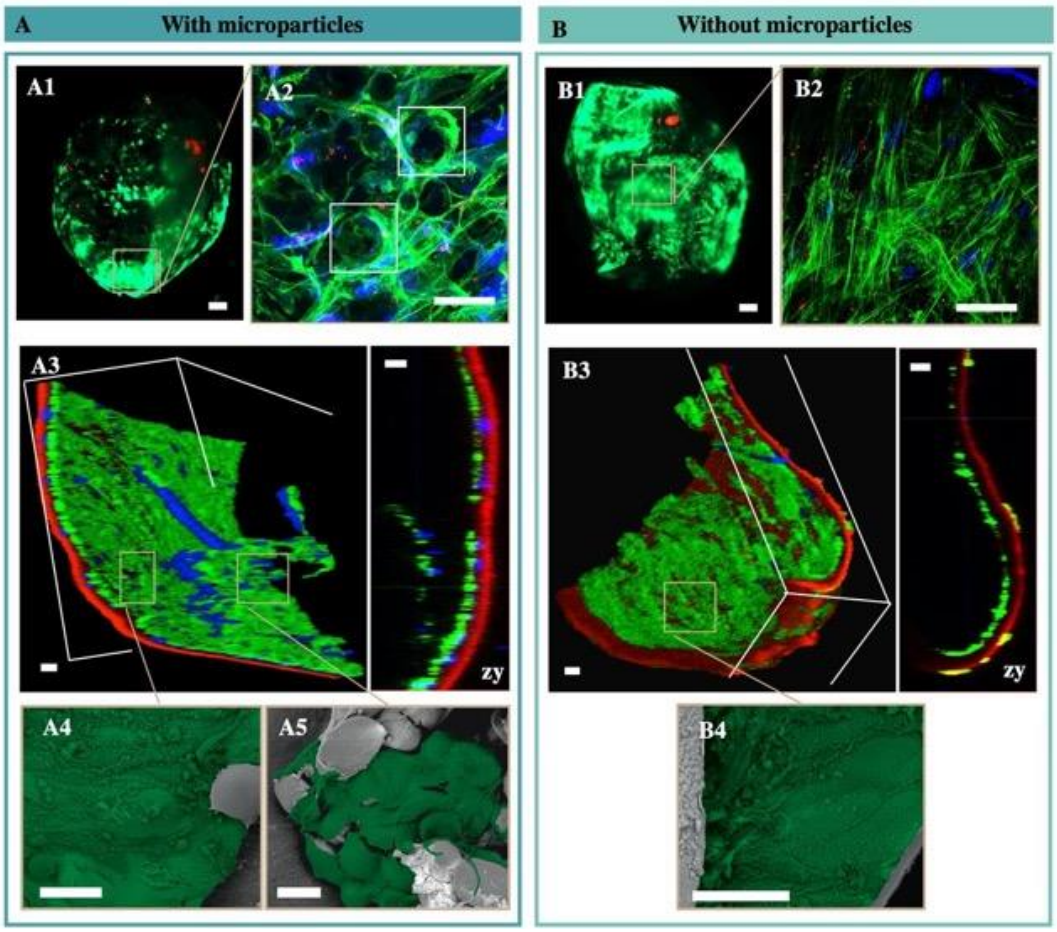

Figure 3. Visualization of the hASC behavior 14 d post-encapsulation in the protein-based liquefied capsules. Overview of the liquefied capsules A) with and B) without the incorporation of microparticles. A1 and A2—fluorescent images of liquefied capsules encapsulating live cells stained with calcein (green) and dead cells stained with propidium iodide (red). Scale bar 200 µm. A2 and B2—CLSM images are displaying the F-actin filaments stained with phalloidin (green) and immunofluorescence of vinculin (red) from cells inside the capsules. A3 and B3—3D reconstruction and orthogonal view of a capsule section with cells stained with phalloidin (green, F-actin microfilaments), DAPI (blue, nucleus) and shell in red (WGA). A4 and B4—SEM images of hASC (green) adhered to the inner shell wall of the capsule with and without the presence of the μPCL, respectively. A5—SEM image of hASC (green) adhered to μPCL (grey). Fluorescent microscopy and SEM images scale bar: 50 µm

(protein-based hydrogel of ≈25 μm thick), we postulate that protein degradation might be starting to occur. Previous studies have reported a time frame of 14–21 days for the degradation of gelatin supports by mesenchymal stem cells, corroborating our findings.[36,37] In the presence of μPCL, no cells were observed outside the shell after the same encapsulation period (14 d), suggesting that the recruitment of the μPCL, delaying the cell/shell interaction, might have contributed to this nonexistence. The presence of only a small number of cells outside the shell membrane may suggest that this behavior require a prior well-established cell ingrowth and proliferation, ensuring an enclosed and protected environment for the first critical days of the tissue formation. Examination of the interior of the capsules by scanning electron microscopy (SEM) validated the interaction cell/shell (Figure 3A4,B4) and cell/μPCL (Figure 3A5). In addition, we can see protrusions along with the interior of the shell (with and without the μPCL) highlighted in green, easily ascribed to the ECM. In contrast, a smooth surface was observed for cell-free liquefied capsules or early encapsulation days (Figure S8A,B, Supporting Information). The production of such a developed ECM before the start of the shell degradation by proteolysis suggests the creation of a "second shell" fashioned by the natural ECM, while allowing formed the tissue to maintain its integrity.

3. Conclusion

Aided by a simple and non-time-consuming methodology, we could fabricate a liquefied system exclusively composed of chemically tailored gelatin. The efficient functionalization with HOPO moieties resulted in a novel oxidation-resistant biomaterial with prevalence for coordination with Fe(III) at physiologic conditions. Moreover, the protein-based shell proved to be a valuable asset working as a bioactive system, providing

the needed adhesion motifs and mechanical support for efficient cell adhesion and proliferation with an evident interaction between cells and

the system. Working as biofactories with a suitable environment to form new tissues, this system also provides cells with the ability to colonize the surrounding environments by the proteolysis of the protein shell and replacement by the natural ECM.

Requiring low in vitro manipulation, this bioactive platform can be used to virtually encapsulate any living cells. With the liquid environment being created at physiological temperatures, we open possibilities using this system as kit-made capsules with the liquefied environments being created only after im- plantation. We believe that this established bioencapsulation system can find excellent application in tissue engineering and regenerative medicine. The exploitation of its biomimetic adhesive properties as building blocks on creating more complex and hierarchical 3D structures could provide a powerful tool with clinical relevance for regenerative therapy.

4. Experimental Section

Reagents and Equipments: Skin porcine gelatin Type A (300 Bloom), ethylenediamine (EDA), Maltol, N-(3-dimethylaminopropyl)-N′- ethylcarbodiimide hydrochloride (EDC) [≥98.0% (AT)], and phosphate buffer saline (PBS) were purchased from Sigma and used without any further purification. Methanol was from Fisher Scientific (p.a., 99.9%). Deuterium chloride [20 wt% solution in deuterium oxide (D_2O, 100.0 atom%)], Sodium deuteroxide (40 wt% solution in D_2O, 99+%) were from Acros. Deuterium Oxide (99.8%) was from TCI Chemicals. For the dialysis, it was used a 3.5 kD MWCO dialysis tubing [45 mm Flat-width, 15 m/roll (50 ft)] from Repligen. Minimum essential medium α-modification (α-MEM), Fetal Bovine Serum, alamarBlue, Live/Dead Kit, 4′,6-diamidino-2-phenylindole dihydrochloride (DAPI), Wheat Germ Agglutinin (WGA)

Alexa Fluor 594 conjugate, and vinculin recombinant rabbit monoclonal antibody were purchased from ThermoScientific (USA). Flash Phalloidin green 488 and Alexa Fluor 594 anti-rabbit (donkey) were purchased from Biolegend (USA).

^{1}H and ^{13}C NMR spectra were recorded using either a Bruker Avance 300 spectrometer at 300.13 and 75.47, respectively or a Bruker Avance 500 at 125.77 MHz for ^{13}C, using D_2O as an internal reference. The chemical shifts are expressed in δ (ppm) and the coupling constants (J) in Hz. The melting point was measured on a Büchi Melting point B-540 apparatus and was uncorrected. The UV–vis spectra and alamarBlue fluorescence were recorded on a Synergy HTX Microplate Reader using a 96-well quartz microplate. Cell viability was with a Zeiss Axio Imager M2, while cell mor- phology by confocal laser scan microscopy (CLSM) using a Zeiss LSM 510 Meta, Zeiss LSM 880 Airyscan, both Carl Zeiss Microscopy GmbH. SEM images were acquired by 25 kV, S4100, Hitachi.

Synthesis of Catechol-Like HOPO-NH_2: Based on a previous procedure with slight modifications,[38] maltol (5.0 g, 39.6 mmol, 1.0 eqv.) and EDA (4.0 mL, 59.4 mmol, 1.5 eqv.) were dissolved in hot distilled water (≈80 °C), and the pH was adjusted to 10 with 6 m HCl solution. After refluxed for 24 h, the reaction mixture was cooled to room temperature (RT) and the water removed under reduced pressure. The crude product was dissolved in 20 mL of distilled water, and its pH brought to ≈7.0 with the addition of 6 m HCl solution. The product was precipitated by methanol addition giv- ing a light brown precipitate isolated by filtration, washed with methanol to yield HOPO-NH_2. Light brown solid, (3.6 g) 54%. mp.: decomposed >275 °C; ^{1}H NMR (300 MHz, D_2O/DCl, δ): 8.04 (d, J = 7 Hz, 1H; ─CH), 7.07(d,J=7Hz,1H;─CH),4.66(t,J=7Hz,2H;─CH_2),3.50(t,J= 7 Hz,

2H; ─CH_2), 2.59 (s, 3H, ─CH_3); ^{13}C NMR (75 MHz, D_2O/DCl, δ): 160.9 (C─OH), 143.4 (C─OH), 141.4 (C2), 138.9 (C5 or C6), 111.7 (C5 or C6), 52.4 (C2′ or C3′), 38.2 (C2′ or C3′), 12.2 (C7); ^{1}H NMR (300 MHz, D_2O,δ):7.65(d,J=7Hz,1H;─CH),6.51(d,J=7Hz,1H;─CH),4.41 (t, J = 6 Hz, 2H; ─CH_2), 3.41 (t, J = 6 Hz, 2H; ─CH_2), 2.42 (s, 3H, ─CH_3); ^{13}C NMR (75 MHz, D_2O, δ): 169.5 (C═O), 145.0 (C─OH), 138.6 (C5 or C6), 134.3 (C2), 112.9 (C5 or C6), 50.8 (C2′ or C3′), 38.6 (C2′ or C3′), 11.5 (C7); ^{1}H NMR (300 MHz, D_2O/NaOD, δ): 7.45 (d, J = 7 Hz, 1H; ─CH), 6.42(d,J=7Hz,1H;─CH),4.08(t,J=6Hz,2H;─CH_2),2.95(t,J= 6 Hz, 2H; ─CH_2), 2.36 (s, 3H, ─CH_3); ^{13} C NMR (75 MHz, D_2 O/NaOD, δ): 170.7 (C═O), 150.2 (C─OH), 135.9 (C5 or C6), 134.8 (C2), 111.8 (C5 or C6), 56.3 (C2′ or C3′), 40.6 (C2′ or C3′), 11.8 (C7).

Synthesis of Gel-HOPO: Type A porcine skin gelatin (1.0 g) was dis- solved in PBS (10 mL, pH 7.4), at 50 °C (≈15 min). The temperature was decreased to 40 °C and the solution pH was brought to ≈8.0. Thereafter, HOPO-NH_2 (0.5 g, 2.97 mmol, in 2 mL PBS) and EDC (0.8 g, 4.17 mmol, in 1 mL PBS) was simultaneously and dropwise added to the gelatin solution. The pH was brought to ≈5.0 with the addition of HCl solution. The reaction was maintained under vigorous stirring at 40 °C for 24 h. After this period, the reaction mixture was dialyzed against 5 L of distilled water at 40 °C, for 3 days (changing the water three times a day). The resulting sample was freeze-dried to yield the Gel-HOPO as a white solid (0.85 g). ^{1}H NMR (300 MHz, D_2O, 40 °C, δ): 7.97 (d, J = 7 Hz, 1H; ─CH), 7.75 (d, J = 7 Hz, 1H; ─CH), 7.46–7.53 (m, 9H, Ar-H-Gel), 7.30 (bs, 1H, Ar-H-Gel), 7.14 (bs, 1H, Ar-H-Gel), 6.98 (bs, 1H, Ar-H-Gel), 6.80 (d, J = 7 Hz, 1H; ─CH), 6.69 (d, J = 7 Hz, 1H; ─CH), 4.55–4.60 (m, 64H; Aliphatic-H-Gel), 4.33–4.37 (m, 40H,

Aliphatic-H-Gel), 4.03–4.14 (m, 127H, Aliphatic-H- Gel), 3.83 (bs, 54H, Aliphatic-H-Gel), 3.41 (bs, 21H, Aliphatic-H-Gel), 3.25 (bs, 14H, Aliphatic-H-Gel), 3.07 (bs, 16H, Aliphatic-H-Gel + $-CH_3$), 2.90 (bs, 10H, Aliphatic-H-Gel), 2.47–2.71 (m, 71H, Aliphatic-H-Gel), 2.20– 2.29 (m, 128H, Aliphatic-H-Gel), 1.87 (bs, 44H, Aliphatic-H-Gel), 1.60 (bd, J = 6 Hz, 59H; Aliphatic-H-Gel), 1.40–1.42 (m, 13H, Aliphatic-H-Gel), 1.12 (bs, 51H, Aliphatic-H-Gel).

HOPO Quantification: Standard solutions of HOPO-NH_2 (0– 20 μg mL^{-1}), Pristine Gelatin and Gel-HOPO (330 μg mL^{-1}) were prepared in distilled water. The calibration curve was obtained by linear regression of the absorbance at 276 nm as a function of the HOPO concentration. Three independent assays were conducted for Gelatin and Gel-HOPO samples. To eliminate any residual interference absorption of gelatin in the quantification process, the Gel-HOPO spectrum values were subtracted from the gelatin spectrum (corrected absorbance spectrum). HOPO concentration in Gel-HOPO was achieved using the resulted calibration curve equation and the Gel-HOPO corrected absorbance at 276 nm.

Preparation of SH: Polystyrene petri dishes were treated according to previous reports.[39] Briefly, a layer of an air-cured coating agent (WX2100, Cytonix) was created onto petri dishes surfaces. After drying for 48 h, the excess of the sprayed solution was removed and submerged in a solution of 70% ethanol for at least 3 days. Afterward, the petri dishes were sterilized into a new 70% ethanol solution overnight, following drying in sterile conditions inside a laminar flow chamber.

Biofabrication Process: The biofabrication of protein-based liquefied capsules is a multi-step process resorting to the SH surfaces. To create the bead, 8 μL of Gel-HOPO (10% w/v in PBS) is dropped onto the SH surface and immediately transferred to 4 °C for a period of ≈1 min. After the gelling process, the beads were transferred to a cold solution of $FeCl_3$ (25 mm in dH_2O, 2 min), washed with cold PBS to remove the excess $FeCl_3$, and transferred to a cold solution of α-MEM (2 min). These three steps were repeated several times for 4, 6, and 8 min in the $FeCl_3$ solution, yielding different shell thicknesses. By the end, the capsules were left in α-MEM and incubated at 37 °C to liquefy the non-coordinated Gel-HOPO.

Morphologic Characterization of the Protein-Based Macrocapsules: The morphologic evaluation of the Gel-HOPO macrocapsules were assessed by optical microscopy. Shell thickness, core, and capsule diameter were assessed by ImageJ image analysis software. Evaluation of the Shell Permeability: Permeability toward cell culture media (α-MEM) was evaluated by simply incubating the newly fabricated capsules overnight at 37 °C. To evaluate bigger molecules, Dextran-FITC with different sizes (20, 40, 75, and 250 kDa) was included in the capsules (10 μL of 5 mg mL^{-1}) by mixing with Gel-HOPO solution and following the biofabrication method. Capsules were then incubated in PBS at 37 °C. At different time points, PBS was collected and replaced by new, fluorescence was read (Ex 485/20 nm, Em 528/20 nm) and plotted as cumulative. The same volume of each Dextran-FITC size was mixed with the same volume of PBS and used as control.

Adhesion Properties of Protein-Based Capsules: To evaluate the adhesion properties, capsules liquefied for a period of 30 min at 37 °C were adhered to different surfaces (glass slides, stainless steel spatula, and skin), ensuring the presence of water, and subjected to

gravity (e.g., turned upside down). Capsule–capsule adhesion was evaluated by pilling capsules in a pyramid shape (resorting to three), or by a more complex construction resorting to a PDMS mold and up to 10 capsules. The integrity of the construction was evaluated over 1 day.

Spherical Microparticles Production and Surface Functionalization: The preparation of microparticles of polycaprolactone (μPCL) were performed as previously described.[10] Succinctly, μPCL were produced by emulsion solvent evaporation technique. A PCL solution (5% w/v) was prepared in dichloromethane and added to a stirring polyvinyl alcohol solution (0.5% w/v), under agitation at RT. After 2 days, the μPCL were collected, washed several times with distilled water, and sieved to obtain a diameter range of 40–50 μm. Then, microparticles were dried with 96% v/v ethanol. Subsequently, the surface was modified by plasma treatment technique. For this, the μPCL were placed into a low-pressure plasma reactor chamber (using atmospheric gas) with low-pressure glow discharge (30 V and 0.2– 0.4 mbar for 15 min) and immediately sterilized with 70% v/v ethanol for 2 h at RT. Afterward, the microparticles were immersed overnight in an acetic acid solution (20 mm) containing collagen I (10 μg cm^{-2}, rat protein tail). Upon preparation and functionalization, the microparticles were kept in PBS and stored at 4 °C. Cell Culture: According to good practice standards, human adipose- derived mesenchymal stem cells (hASCs) were isolated from adipose tissue following informed consent and patient anonymization. The retrieval and transportation of the samples to the laboratorial facilities was performed under a protocol previously established between the COMPASS research group (University of Aveiro) and the Hospital da Luz (Aveiro, Portugal), which was approved by the hospital Ethical Committee.

Production of the Cell Loaded Protein-Based Capsules: hASC (passages between P5 and P7) were cultured in α-MEM supplemented with FBS (10% v/v) and antibiotic–antimycotic (1% v/v). At ≈80% cells were detached using trypsin-EDTA at 37 °C and centrifuged at 300 g for 5 min. Cells (2 000 000 per mL) were then suspended in a solution containing Gel-HOPO (10% w/v in 1× DPBS). The biofabrication of the capsules was accomplished as previously described, using a total of 6 min incubation in the cold $FeCl_3$ solution. For the capsules containing microparticles, μPCL (20 mg mL^{-1}) were included in the cells and Gel-HOPO suspension followed by the common biofabrication process.

Cell Viability Assay: Cell viability was evaluated by live-dead fluorescence assay according to the manufacture's recommendation. Briefly, at 1, 7, and 14 d post-encapsulation, capsules with and without the μPCL were washed in immersed in 1× Dulbecco's phosphate-buffered saline (DPBS) and then stained with calcein-AM and propidium iodide for 20 min at 37 °C. Afterward, samples were immediately visualized by fluorescence microscopy.

Mitochondrial Metabolic Activity: Mitochondrial metabolic activity quantification (n = 3) was performed at 1, 3, 7, and 14 days using the alamarBlue cell viability according to the manufacturer's specifications. Encapsulated cells were incubated overnight at 37 °C with 10% (v/v) of the reagent, and the fluorescence (Ex: 540/35 nm, Em: 600/40 nm) measured with a microplate reader.

Evaluation of F-Actin Filaments and Vinculin Expression: The entire protocol was performed at RT unless otherwise indicated. Capsules were fixed with 4% paraformaldehyde in 1× PBS for 30 min, washed in PBS and permeabilized with 0.1%

Triton X-100 in 1× PBS for 5 min. After that, samples were blocked with 1% BSA in 1× PBS for 30 min and incubated overnight at 4 °C with vinculin recombinant rabbit monoclonal antibody (1:50). After washing with 1× PBS, encapsulated cells were double-stained with Alexa Fluor 594 anti-rabbit (donkey) (1:400) for the vinculin, and Flash Phalloidin Green 488 (1:40) for F-actin filaments for 60 min. After washing with 3× PBS, the shell was stained with WGA (5.0 μg mL^{-1}) for 30 min at RT. Nuclei counterstaining was performed by incubating capsules with DAPI (1 mg mL^{-1} diluted 1:1000) for 5 min, followed by washing with 1× PBS. Capsules were further analyzed by confocal laser scanning microscopy (CLSM).

Scanning Electron Microscopy: Capsules were fixed at RT in paraformaldehyde (10% v/v) for 30 min and subsequently dehydrated in increasing gradient series of ethanol (10 min each). The shell of the capsules was destroyed to expose the core contents. After carbon sputtering, samples were visualized.

Statistical Analysis: All statistical data was conducted using GraphPad Prism v6.0 software. Results are expressed as mean ± SD. For the evaluation of the capsule morphology n = 8, for the analysis of shell permeability n = 5, and for the metabolic activity n = 4. The statistical analysis was performed using two-way ANOVA test, followed by a Tukey's multiple comparisons test for pairwise comparison. Statistical significances were established for p-values < 0.05. The results are not significant unless otherwise marked with an asterisk character (*).

Supporting Information

Supporting Information is available from the Wiley Online Library or from the author.

Acknowledgements

The authors acknowledge the support of the European Research Council for project ATLAS, grant agreement ERC-2014-ADG-669858. This work was developed within the scope of the project CICECO-Aveiro Institute of Mate- rials, UIDB/50011/2020 & UIDP/50011/2020, financed by national funds through the FCT/MEC and when appropriate co-financed by FEDER under the PT2020 Partnership Agreement. This work was also supported by the Programa Operacional Competitividade e Internacionalização (POCI), in the component FEDER, and by national funds (OE) through FCT/MCTES, in the scope of the projects BEAT (PTDC/BTM-MAT/30869/2017) and MARGEL (PTDC/BTM-MAT/31498/2017). The Beat and MARGEL projects are acknowledged for the individual Junior Researcher contracts of M.C.G. and D.C.S.C., respectively. The ATLAS project is acknowledged for the post- doctoral fellowship of C.S.O. M.C.G. also acknowledges BioRender.com.

Conflict of Interest

The authors declare no conflict of interest.

References

[1] V. M. Gaspar, P. Lavrador, J. Borges, M. B. Oliveira, J. F. Mano, Adv. Mater. 2020, 32, 1903975.

[2] C. R. Correia, S. Nadine, J. F. Mano, Adv. Funct. Mater. 2020, 30, 1908061.

[3] B.Kupikowska-Stobba,D.Lewinska,Biomater.Sci.2020,8,1536.

[4] H.Domejean,M.delaMotteSaintPierre,A.Funfak,N.Atrux-Tallau, K. Alessandri, P. Nassoy, J. Bibette, N. Bremond, Lab Chip 2016, 17, 110.

[5] V. Kozlovskaya, J. Chen, O. Zavgorodnya, M. B. Hasan, E. Kharlampieva, Langmuir 2018, 34, 11832.

[6] R.R.Esfahani,H.Jun,S.Rahmani,A.Miller,J.Lahann,ACSOmega 2017, 2, 2839.

[7]C.R.Correia,R.L.Reis,J.F.Mano,Biomacromolecules2013,14,1250.

[8] B.C.Zarket,S.R.Raghavan,Nat.Commun.2017,8,193.

[9] S. Vilabril, S. Nadine, C. Neves, C. R. Correia, M. G. Freire, J. A. P. Coutinho, M. B. Oliveira, J. F. Mano, Adv. Healthcare Mater. 2021, 10, 2100266.

[10] S. Nadine, S. G. Patricio, C. R. Correia, J. F. Mano, Biofabrication 2019, 12, 015005.

[11] M. C. Gomes, J. F. Mano, Biomater. Biosyst. 2021, 1, 100010.

[12] K. Lin, D. Zhang, M. H. Macedo, W. Cui, B. Sarmento, G. Shen, Adv. Funct. Mater. 2019, 29, 1804943.

[13] S. C. Santos, C. A. Custodio, J. F. Mano, Adv. Healthcare Mater. 2018, 7, 1800849.

[14] W. Zhang, R. Wang, Z. Sun, X. Zhu, Q. Zhao, T. Zhang, A. Cholewinski, F. K. Yang, B. Zhao, R. Pinnaratip, P. K. Forooshani, B. P. Lee, Chem. Soc. Rev. 2020, 49, 433.

[15] S. Azevedo, A. M. S. Costa, A. Andersen, I. S. Choi, H. Birkedal, J. F. Mano, Adv. Mater. 2017, 29, 201700759.

[16] A. H. J. Gowda, Y. Bu, O. Kudina, K. V. Krishna, R. A. Bohara, D. Eglin, A. Pandit, Int. J. Biol. Macromol. 2020, 164, 1384.

[17] J. Fu, K. Y. Quek, Y. J. Chuah, C. S. Lim, C. Fan, D. A. Wang, J. Mater. Chem. B 2016, 4, 7961.

[18] X. Zhao, M. Zhang, B. Guo, P. X. Ma, J. Mater. Chem. B 2016, 4, 6644.

[19] M. S. Menyo, C. J. Hawker, J. H. Waite, Soft Matter 2013, 9, 10314.

[20] A. Andersen, M. Krogsgaard, H. Birkedal, Biomacromolecules 2018, 19, 1402.

[21] A. M. Costa, J. F. Mano, J. Am. Chem. Soc. 2017, 139, 1057.

[22] P. B. Pansuriya, M. N. Patel, J. Enzyme Inhib. Med. Chem. 2008, 23, 230.

[23] M. Krogsgaard, M. R. Hansen, H. Birkedal, J. Mater. Chem. B 2014, 2, 8292.

[24] T. Watanabe, I. Motohiro, T. Ono, Langmuir 2019, 35, 2358.

[25] S. Zhao, P. Agarwal, W. Rao, H. Huang, R. Zhang, Z. Liu, J. Yu, N. Weisleder, W. Zhang, X. He, Integr. Biol. 2014, 6, 874.

[26] S. Nadine, S. G. Patricio, C. C. Barrias, I. S. Choi, M. Matsusaki, C. R. Correia, J. F. Mano, Adv. Biosyst. 2020, 4, 2000127.

[27] A. M. Costa, J. F. Mano, Chem. Commun. 2015, 51, 15673.

[28] M. L. Chou, T. Burnouf, T. J. Wang, PLoS One 2014, 9, e99145.

[29] B. A. Yang, T. M. Westerhof, K. Sabin, S. D. Merajver, C. A. Aguilar, Adv. Sci. 2021, 8, 2002825.

[30] J. Saiz-Poseu, J. Mancebo-Aracil, F. Nador, F. Busque, D. Ruiz-Molina, Angew. Chem., Int. Ed. Engl. 2019, 58, 696.

[31] A. I. Neto, N. L. Vasconcelos, S. M. Oliveira, D. Ruiz-Molina, J. F. Mano, Adv. Funct. Mater. 2016, 26, 2745.

[32] Q. Li, Y. W. Zhang, C. F. Wang, D. A. Weitz, S. Chen, Adv. Mater. 2018, 30, 1803475.

[33] F. Li, V. X. Truong, P. Fisch, C. Levinson, V. Glattauer, M. Zenobi-Wong, H. Thissen, J. S. Forsythe, J. E. Frith, Acta Biomater. 2018, 77, 48. [34] C. R. Correia, I. M. Bjorge, J. Zeng, M. Matsusaki, J. F. Mano, Adv. Healthcare Mater. 2019, 8, 1901221.

[35] K. A. Jansen, P. Atherton, C. Ballestrem, Semin Cell Dev. Biol. 2017, 71, 75.

[36] L. D. Solorio, L. M. Phillips, A. McMillan, C. W. Cheng, P. N. Dang, J. E. Samorezov, X. Yu, W. L. Murphy, E. Alsberg, Adv. Healthcare Mater. 2015, 4, 2306.

[37] S. Herberg, D. Varghai, D. S. Alt, P. N. Dang, H. Park, Y. Cheng, J. Y. Shin, A. D. Dikina, J. D. Boerckel, M. W. Rolle, E. Alsberg, Commun. Biol. 2021, 4, 89.

[38] Y. Mawani, J. F. Cawthray, S. Chang, K. Sachs-Barrable, D. M. Weekes, K. M. Wasan, C. Orvig, Dalton Trans. 2013, 42, 5999.

[39] A. R. Sousa, C. Martins-Cruz, M. B. Oliveira, J. F. Mano, Adv. Mater. 2020, 32, 1906305.

Supporting Information

Design of protein-based liquified cell-laden capsules with bioinspired adhesion for tissue engineering

Maria C. Gomes, Dora C. S. Costa, Cláudia S. Oliveira, João F. Mano**

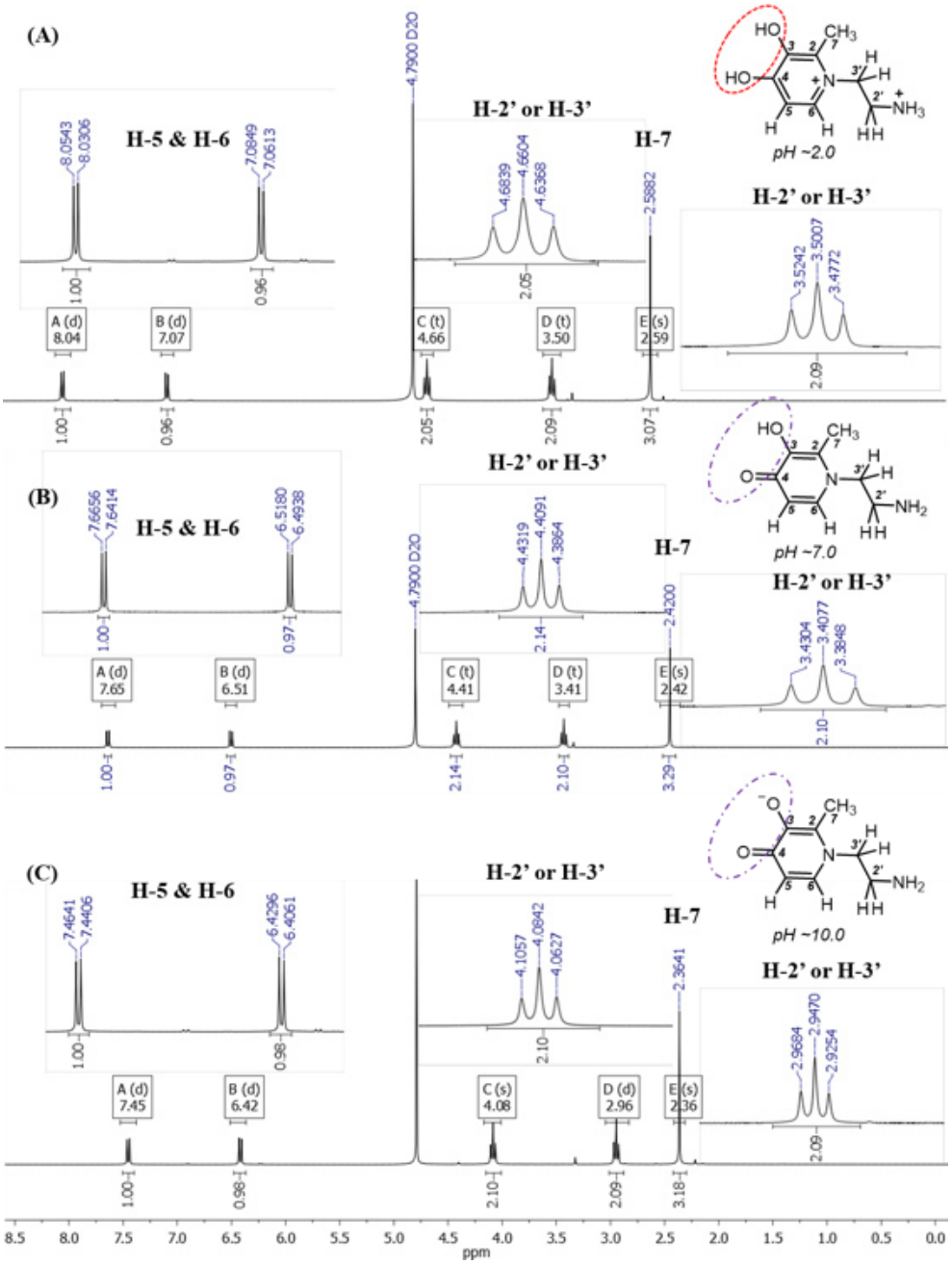

Figure S1. Comparative ^{1}H NMR Spectra (300.0 MHz) of HOPO-NH_2 (3) at (A) pH ~2.0 (D_2O/DCl), (B) pH~7.0 (D_2O) and (C) pH~10.0 (D_2O/NaOD).

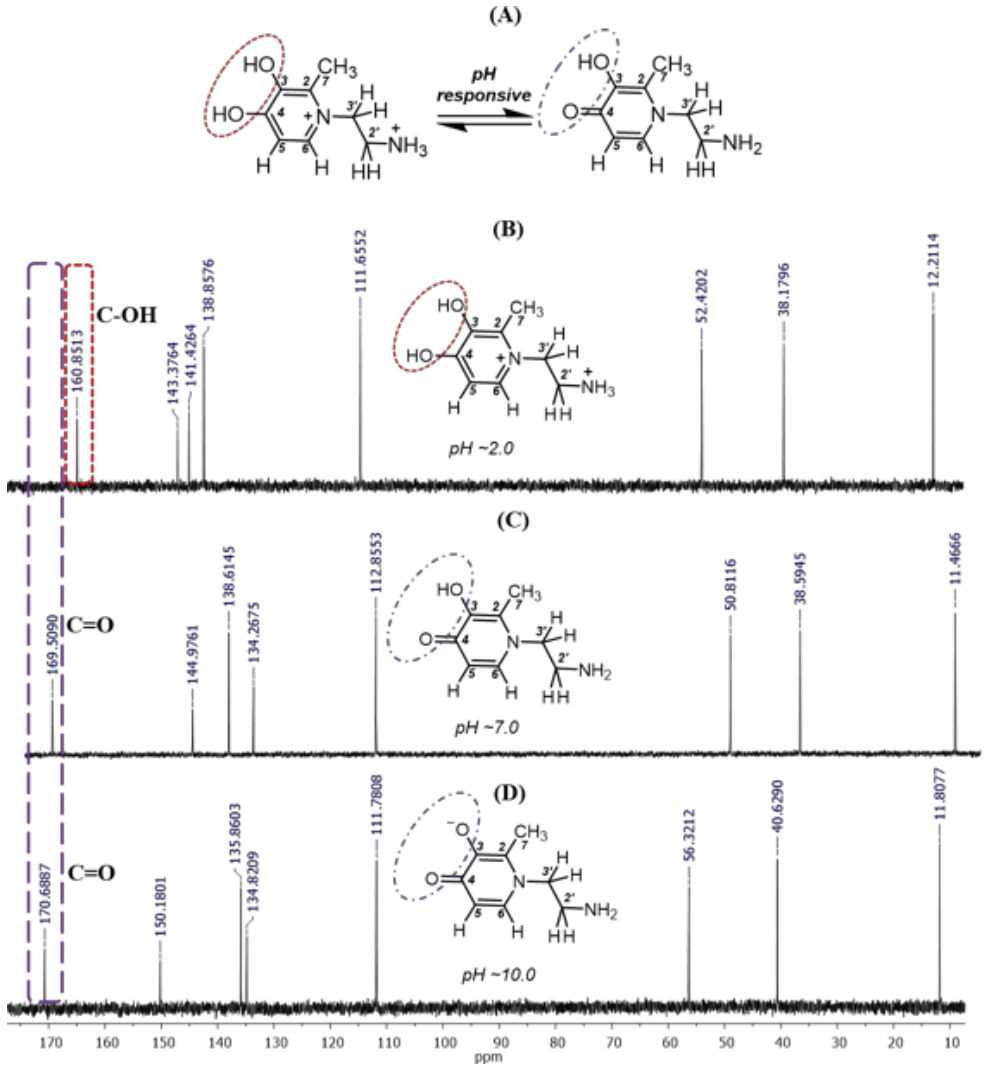

Figure S2. (A) Equilibrium scheme of HOPO-NH_2 (3) tautomers and Comparative ^{13}C NMR Spectra (75.0 MHz,) of 3 at (B) pH ~2.0 (D_2O/DCl), (C) pH~7.0 (D_2O) and (D) pH~10.0 (D_2O/NaOD).

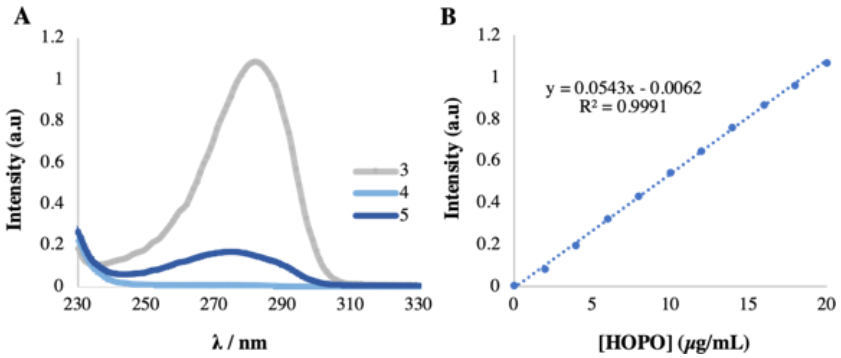

Figure S3. A) Normalised (at 210 nm) UV-Vis Spectra of HOPO-NH_2, pristine Gelatin and Gel-HOPO in distilled water. B) Standard curve (abs 276 nm) of HOPO (0-20 µg/mL) in distilled water.

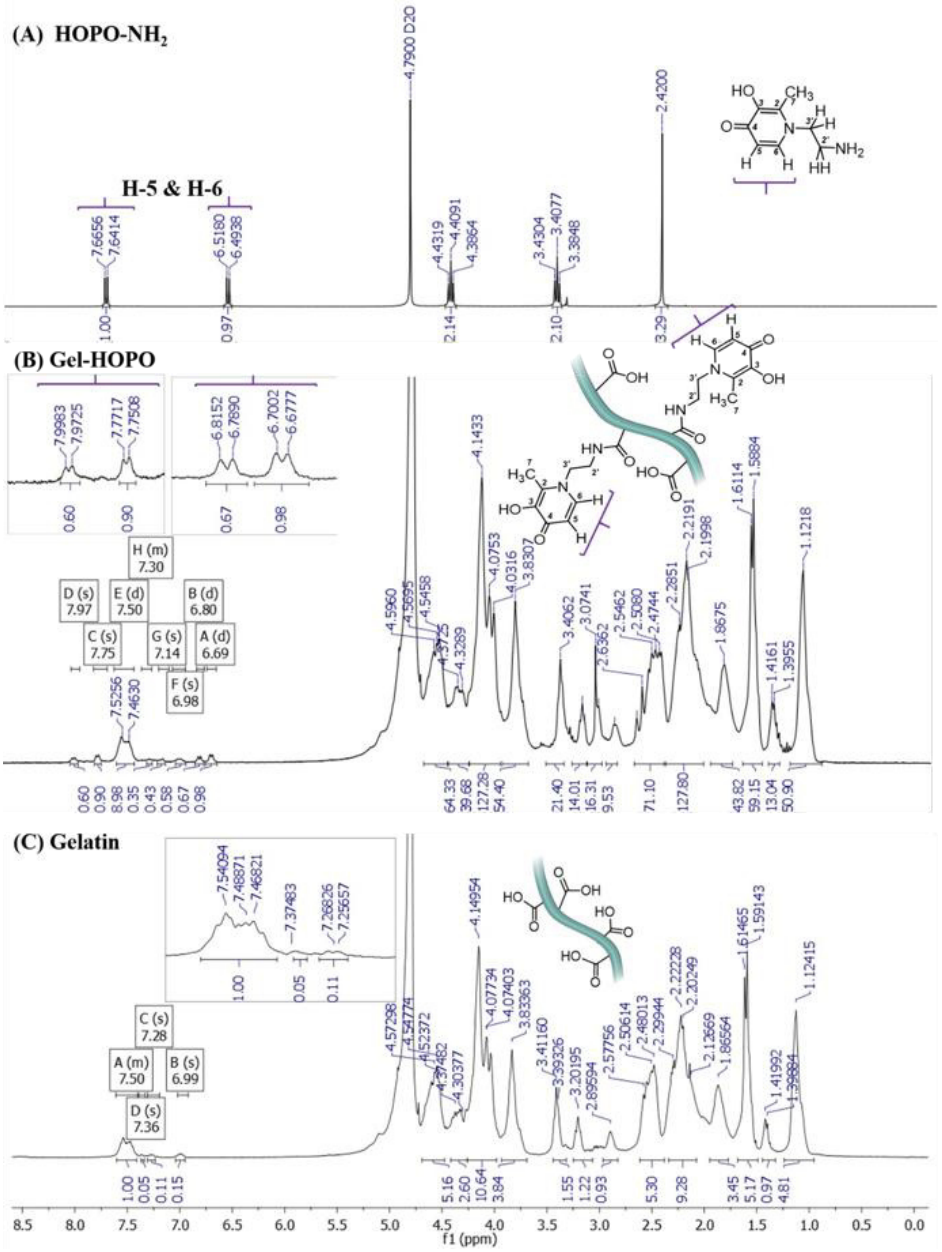

Figure S4. ^{1}H NMR spectra (D_2O, 300.0 MHz, 40 oC, pH ~7.0) of (A) HOPO-NH_2 (3), (B) Gel-HOPO (5) and (C) Gelatin (4).

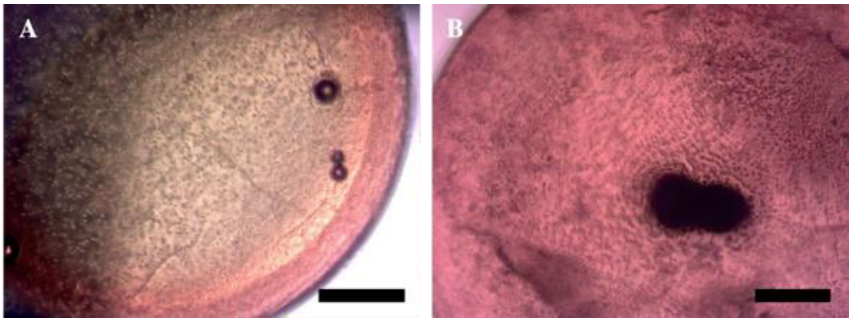

Figure S5 hASC distribution after encapsulation in the Gel-HOPO capsules A) before and B) core liquefaction at 37 oC. Scale bar 200 µm.

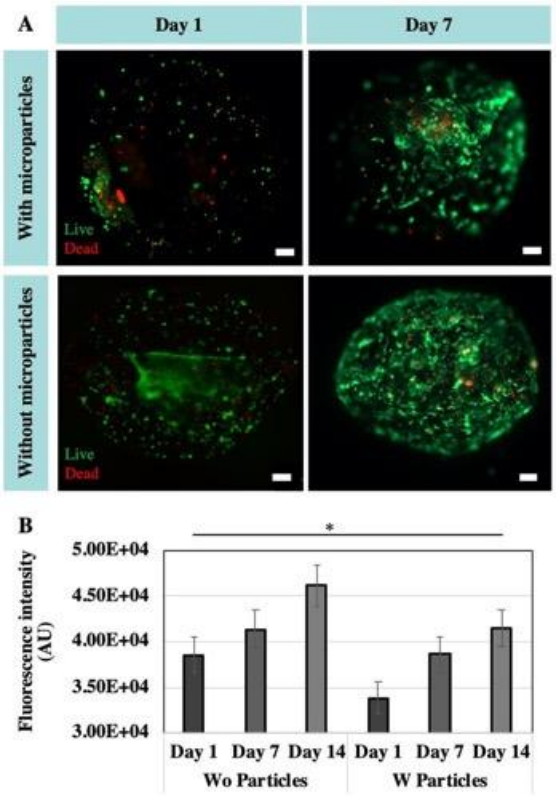

Figure S6 A) fluorescent imagens of liquified capsules encapsulating live cells stained with calcein (green) and dead cells stained with PI (red). Scale bar 200 µm. B) Metabolic activity measured by AlamarBlure® fluorescent assay. Scale bar 200 µm. Data is presented as mean ± SD, n= 4. Statistical analysis was performed by two-way ANOVA with Tukey's post-test; statistically significant considered for * $p < 0.05$

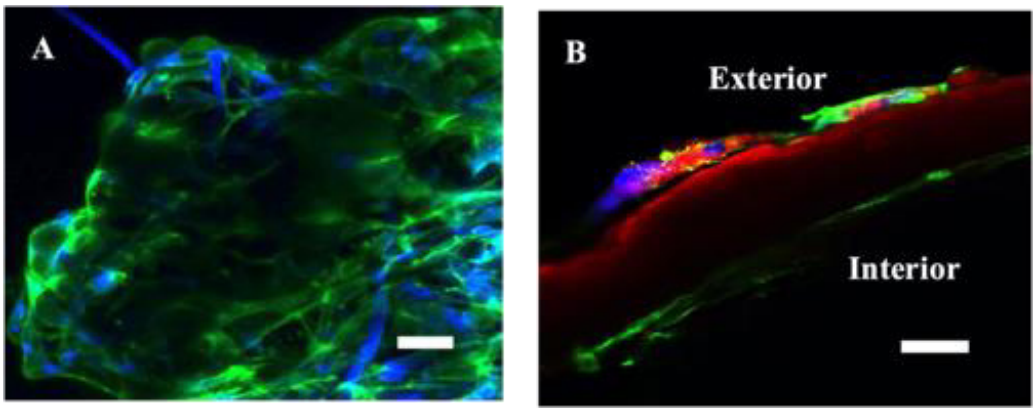

Figure S7 LSCM images displaying the hASC interaction after 14 d post-encapsulation with A) the μPCL and B) the shell exterior. F-actin filaments were stained with phalloidin (green), nuclei with DAP (blue) and capsule shell with WGA (red). Scale bar: 50 μm.

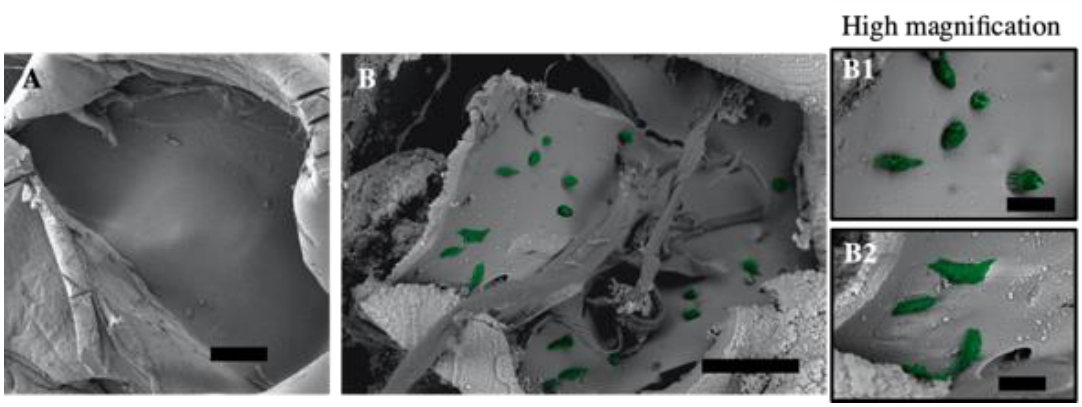

Figure S8 SEM imagens displaying the inner shell morphology present in the liquified capsules A) without cells and B) after 1 d post hASC encapsulation. High magnification imagens exposing B1) early cells adhesion and B)2 full spread along the inner shell. Scale bars A) and B) 100 μm, B1 and B2 25 μm.